Semnan University

Journal of Heat and Mass Transfer Research

Journal homepage: https://jhmtr.semnan.ac.ir

ISSN: 2383-3068

Research Article

Viscous Dissipation and Chemical Reaction on Radiate MHD Casson Nanofluid Past a Stretching Surface with a Slip Effect

Dachapally Swapna [a], Kamatam Govardhan [b], Ganji Narender [c *], Santoshi Misra [d]

[a] *Department of Mathematics, Osmania University College for Women, Koti, Hyderabad, Telangana, India.*
[b] *Department of Mathematics, GITAM University, Hyderabad, Telangana, India.*
[c] *Department of Humanities and Sciences (Mathematics), CVR College of Engineering, Hyderabad, Telangana, India.*
[d] *Department of Mathematics, St. Ann's College for Women, Hyderabad, Telangana, India.*

ARTICLE INFO

Article history:

Received: 2023-09-10

Revised: 2024-01-04

Accepted: 2024-01-04

Keywords:

MHD;
Casson nanofluid;
Viscous dissipation;
Chemical reaction;
Shooting technique;
Adams – Moulton method.

ABSTRACT

This article explains the MHD Casson nanofluid flow in the presence of chemical reaction coefficient past a linear stretching surface along with the slip condition. Mainly, the analysis of heat and mass transfer in the presence of Brownian motion and the thermophoretic diffusion effect is performed. Mathematical modeling for the law of conservation of mass, momentum, hear and concentration of nanoparticles is executed. Governing nonlinear partial differential equations are transformed into the dimensionless nonlinear ordinary differential equations by using appropriate transformations. To achieve numerical solution for the considered model, shooting technique and Adams-Moulton method of fourth order are used to obtain the numerical results via the computational program language FORTRAN. Comparison between the obtained results and previous works are well in agreement was observed. For the velocity, temperature, and concentration profiles, numerical computations are conducted. The effects slip parameter, velocity ratio parameter, Casson parameter, Casson parameter taken the problem. Numerical values of the local skin-friction, Nusselt number and nanoparticle Sherwood number are computed and analyzed. It is noted that the skin-friction coefficient decreases for the larger values of velocity ratio parameter, slip parameter, and increases with an increasing value of Casson parameter. It is also found that enhancing the chemical reaction parameter leads to decrease in concentration profile. In addition, physical quantities of absorption like skin friction, local Nusselt and Sherwood numbers are also shown graphically.

1. Introduction

In the last few years, the non-Newtonian fluids attracted the attention of the mathematicians, physicist, engineers, etc., due to their demanding applications of domestic and industrial usage. In our daily life such applications are all around us, from a morning coffee to an evening bath. Such applications include toothpaste, paints, gels, lubrication oils, polymers, etc., The Navier Stokes equations due to their composite structure, cannot effectively describe the flow of non-Newtonian fluids. In the non-Newtonian fluids, the constitutive equations exist much more complex than the Navier Stokes equations. There is no one constitutive equation that can be used to study all non-Newtonian fluids, explaining the complex behavior of fluids. Some relevant studies

* **Corresponding author.**
E-mail address: gnriimc@gmail.com

Cite this article as:
Swapna, D., Govardhan, K., Narender, G. and Misra, S., 2023. Viscous Dissipation and Chemical Reaction on Radiate MHD Casson Nanofluid Past a Stretching Surface with a Slip Effect. *Journal of Heat and Mass Transfer Research*, 10(2), pp. 315 - 328.
https://doi.org/10.22075/JHMTR.2024.31758.1477

about non-Newtonian fluids can be seen from the list [1,2].

Casson fluid is discussed under the class of non-Newtonian fluids. Shortcomings of the Bingham fluid model is countered by this model as it explains the nonlinear behavior seen once the yield stress is achieved. The Casson fluid model successfully explains the physical behavior of many fluids used in science and industry. For instance, in chocolate manufacturing industry, the quality of chocolate products depend on the viscosity of the chocolate. Chocolate shows a shear thinning behavior which is explained best by the Casson fluid model [3]. Narender et al. [4] studied the impact of the radiation effects in the presence of heat generation/absorption and magnetic field on the magnetohydrodynamics (MHD) stagnation point flow over a radially stretching sheet using a Casson nanofluid. The method employed by the authors is the shooting method with Adams – Moulton method. Narender et al. [5] explored the impacts of external magnetic field inclinations and viscous dissipation due to heat generation or absorption parameter on MHD mixed convective flow of Casson nanofluid. They found that with an increase in Casson parameter, the velocity field is suppressing, in parallel with an increase in Casson parameter temperature raised. A work was done by Govardhan et al. [6] on heat transfer with MHD Casson fluid flow towards a linear stretching sheet with temperature distribution over the sheet. The authors found out that solution depends on Brownian motion number, thermophoresis number, Prandtl number. Sime recent studies on heat transfer and nanofluid flows are presented in Elelamy, A.F. et al. [7], M.A. Yousif et al. [8] and Zeeshan, A. et al. [9] did a piece of work on nanofluid in a stretching sheet in which MHD flow is investigated. The problem was solved by a numerical technique.

Besides, the study of magnetohydrodynamic flow has gained the attention of modern era scientists on account of its extensive industrial and engineering application. Such applications incorporate the design of cooling frameworks by including liquid metals, MHD generators, petroleum industries, accelerators, nuclear reactors, energy stockpiling, pumps, gas turbines and flow meters. Having such an idea as a top priority the scientists and mathematician investigated the behavior of MHD flows in different physical angles. Sheikholeslami et al. [10] scrutinized the properties of magnetohydrodynamic nanofluid. The method employed by the authors is the lattice Boltzmann method. The MHD flow of nanofluid provoked by a stretching surface was examined by Rashidi et al. [11]. They found that magnetic fields lead to decrease the nanofluid velocity and increase the nanofluid temperature. Zeeshan et al. [12] inspected the results of magnetic dipole on ferrofluid. They discussed the problem physically for various flow problems. Hayat et al. [13] inspected the consequences of Jeffrey fluid model with convective boundaries. Narender et al. [14] examined the viscous dissipation and thermal radiation effects on the MHD mixed convection stagnation point flow of Maxwell nanofluid over a stretching surface. In this area, various studies have been performed [15,16].

Thermal radiation is conducted through electromagnetic waves. The energy is transferred due to temperature difference between the two surfaces. In this process the energy is spread in the form of waves in all directions. The emission of these radiations depends on temperature surface, nature of surface and frequency of radiations. If the temperature difference is small then linear thermal radiation is applicable, however if the difference of temperature is large then linear thermal radiation is not applicable. In recent years, many researchers focused on the utilization of magnetohydrodynamics along with the thermal radiation phenomenon to study the heat and mass transfer analysis due to its diversified applications. S. Shah et al. presented numerical analysis of Cattaneo-Christov heat flux model for MHD flow of Maxwell fluid with thermal radiation [17].

The Shooting method and the MATLAB built in routine bvp4c applied for computing solutions. The thermal characterization of two-dimensional Maxwell nanofluid flow over a permeable stretching sheet using the finite element method was investigated by Madhu et al. [18]. Thermal radiation influences in various fluids with the imposition of different conditions is studied by Endalew and Nayak [19].

The chemical reaction stimulus a great role in the investigation involving heat and mass in areas of science and engineering technology. Zhang et al. [20] studied the effects of chemical reaction and thermal radiation on nanofluids of heat transfer through the porous medium. Sarma et al. [21] considered the problem as a boundary layer flow over a stretching sheet with chemical reaction.

A chemical reaction between the conventional liquid and nanoparticles are classified as a homogeneous reaction during a given phase or heterogeneous reaction i.e., surrounded by a boundary of phase. Reaction rate in the first order chemical reaction is straightly related to the concentration. Several authors examined the effect of chemical reaction on nanofluids of heat transfer over a stretching sheet [22 – 24].

The novelty of the present study rests upon the following. The study takes care of the

nanofluid flow with Cassion fluid as the base fluid and suspended nanoparticles. Important mechanisms such as thermophoresis and Brownian motion effect emphasizes the nanoparticle characteristics. The existing model is mathematically formulated to the system of nonlinear partial differential equations and converted into system of coupled nonlinear nonlinear ordinary differential equations via similarity invariants. A numerical solution of the system of ODEs is obtained by employing the shooting method and Adams Moulton method of fourth order the precision of the obtained numerical results is compared by using the computational program FORTRAN code. The objective is to simulate the effect of important parameters on flow, heat, and mass transfer phenomena. To the best of the authors knowledge, this is the first study to investigate a mathematical model with numerical simulation.

2. Mathematical Modelling

Consider the 2-D stagnation point flow of MHD Casson fluid over a stretching surface under the impact of slip wall. Magnetic field of strength is applied B_0 perpendicular to the fluid motion. Additionally, the impacts of Brownian motion and thermophoretic diffusion are also considered. Furthermore, the equations of energy and mass transport are known to determine the profiles of heat and concentration, respectively. At $x-$axis the stretching sheet is taken and $y-$axis is normal to the plate that can be seen in Figure 1. The stretching and slip velocities at the boundary are taken as $U_w(x)=a\,x$ and $U_{slip}=\left(\mu_B+\frac{P_y}{\sqrt{2\pi_c}}\right)\frac{\partial u}{\partial y}$ respectively, where p_y denotes the yield stress, T_w is the surface temperature, μ_B is the plastic dynamic viscosity, π_c represents the critical value of product, $U_\infty=b\,x$, T_∞, C_∞ represent the free stream velocity, temperature, and concentration.

Governing Equations:

The elementary governing equations are shown as follows for the two-dimensional incompressible Casson nanofluid [25]:

$$\frac{\partial u}{\partial x}+\frac{\partial v}{\partial y}=0, \tag{1}$$

$$\left.\begin{aligned} u\frac{\partial u}{\partial x}+v\frac{\partial u}{\partial y}=\nu\left(1+\frac{1}{\gamma}\right)\frac{\partial^2 u}{\partial y^2}+U_\infty\frac{\partial U_\infty}{\partial x}\\ +\frac{\sigma B_0^2}{\rho_f}(U_\infty-u), \end{aligned}\right\} \tag{2}$$

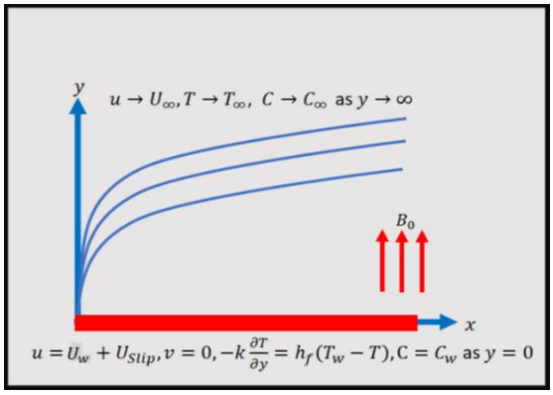

Fig. 1. Geometrical view of the Physical mode.

$$\left.\begin{aligned} u\frac{\partial T}{\partial x}+v\frac{\partial T}{\partial y}=\alpha\frac{\partial^2 T}{\partial y^2}+\Gamma\left\{D_B\frac{\partial C}{\partial y}\frac{\partial T}{\partial y}+\frac{D_T}{T_\infty}\left(\frac{\partial T}{\partial y}\right)^2\right\}\\ -\frac{1}{(\rho C)_f}\frac{\partial q_r}{\partial y}+\frac{\nu}{C_p}\left(1+\frac{1}{\gamma}\right)\left(\frac{\partial u}{\partial y}\right)^2, \end{aligned}\right\} \tag{3}$$

$$\left.\begin{aligned} u\frac{\partial C}{\partial x}+v\frac{\partial C}{\partial y}=D_B\frac{\partial^2 C}{\partial y^2}+\frac{D_T}{T_\infty}\frac{\partial^2 T}{\partial y^2}\\ -K^{\bullet}(C-C_\infty). \end{aligned}\right\} \tag{4}$$

The related BCs can be described as [25]:

$$\left.\begin{aligned} &\text{Wall conditions}\,(y=0):\\ &u=U_w(x)+U_{Slip}\Rightarrow u=ax+\left(\mu_B+\frac{P_y}{\sqrt{2\pi_c}}\right),\\ &v=0,\ -k\frac{\partial T}{\partial y}=h_f(T_f-T),\ C=C_w.\\ &\text{Free stream conditions}\,(y\to\infty):\\ &u\to U_\infty=b\,x,\ v=0,\ T\to T_\infty,\ C\to C_\infty. \end{aligned}\right\} \tag{5}$$

here, u and v represent the velocity elements in the direction of $x-$axis and $y-$axis respectively, ρ_f is the fluid density, σ denotes the electrical conductivity, T represents the temperature, α is the thermal diffusivity, Γ represents the relation among heat capacity of the antiparticle and the liquid, C is the concentration parameter, μ_B represents the dynamic viscosity, p_y denotes the yield stress, π_c represents the critical value of product and a, b are positive constants. As the heat flux is transported to the body as conduction, the following boundary condition holds good.

$$-k\frac{\partial T}{\partial y}=h_f\left(T_f-T\right)$$

Here, k denotes the thermal conductivity, h_f denotes the coefficient of heat transfer.

3. Similarity Transformation

The following similarity variables for translation of PDEs into ODEs have been added here.

$$\left.\begin{aligned} &\eta = y\sqrt{\frac{a}{\nu}}, \qquad \psi = \sqrt{a\,\nu}\,x\; f\;(\eta),\\ &\theta(\eta) = \frac{T - T_\infty}{T_w - T_\infty},\;\; \phi(\eta) = \frac{C - C_\infty}{C_w - C_\infty}. \end{aligned}\right\} \quad (6)$$

The above, equation (1) is satisfied identically. The equations take the form after employing similarity transformation.

$$\left(1+\frac{1}{\gamma}\right) f''' + ff'' - \left(f'\right)^2 + A^2 + M\left(A - f'\right) = 0, \quad (7)$$

$$\left(1+\frac{4}{3R}\right)\theta'' + \Pr\left(\begin{aligned} &f\theta' + Ec\left(1+\frac{1}{\gamma}\right)\left(f''\right)^2\\ &+Nb\;\phi'\theta' + Nt\left(\theta^1\right)^2 \end{aligned}\right) = 0, \quad (8)$$

$$\phi'' + Le\;\Pr\;\phi' + \frac{Nt}{Nb}\theta'' - Le\;Kr\;\phi = 0. \quad (9)$$

The dimensionless conditions associated with the boundary are as follows:

$$\left.\begin{aligned} &f(\eta) = 0,\\ &f'(\eta) = 1 + \delta\left(1+\frac{1}{\gamma}\right)f''(\eta),\\ &\theta'(\eta) = -Bi\left[1 - \theta(\eta)\right],\\ &\phi(0) = 1 \end{aligned}\right\}, at\;\eta = 0,$$
$$\left.\begin{aligned} &f'(\eta) \to A, \quad \theta(\eta) \to 0,\\ &\phi(\eta) \to 0 \end{aligned}\right\} as \quad \eta \to \infty \quad (10)$$

in the above equation δ momentum slip parameter, A the ratio of stretching velocity of free stream and lower plate. The temperature field is dependent on Biot number (Bi) when the heat transfer takes places into the fluid.

The following expression refers to different parameters used in the above equations [20]:

$$\left.\begin{aligned} &Bi = \frac{h_f}{k}\sqrt{\frac{\nu}{a}},\; R = \frac{4\sigma^* T_\infty^3}{k_0 k}, M = \frac{\sigma B_0^2(x)}{\rho_f a},\\ &Ec = \frac{u^2}{C_p(T_f - T_\infty)},\; A = \frac{b}{a},\; \delta = \mu_B\sqrt{\frac{a}{\nu}}\\ &Nb = \frac{(\rho C)_p}{(\rho C)_f \nu} D_B (C_w - C_\infty),\; L_e = \frac{\alpha}{D_B}\\ &Nt = \frac{(\rho C)_p}{(\rho C)_f \nu} D_T (T_w - T_\infty), \quad \Pr = \frac{\nu}{\alpha}. \end{aligned}\right\} \quad (11)$$

The physical quantities which govern the flow are the Nusselt number (Nu_x), Sherwood number (Sh_x) and skin friction coefficient (C_f), which are given by,

$$\left.\begin{aligned} &Nu_x = \frac{xq_w}{k(T_w - T_\infty)},\\ &Sh_x = \frac{xh_m}{D_B}(C_w - C_\infty), \qquad C_f = \frac{\tau_w}{\rho u_w^2} \end{aligned}\right\} \quad (12)$$

where heat, mass flux at the surface are q_w and h_m respectively defined as $q_w = -k\left(\frac{\partial T}{\partial y}\right)$, $h_m = -D_B\left(\frac{\partial \phi}{\partial y}\right)$ and the skin - friction on flat plate τ_w is given by $\tau_w = \left(\mu_B + \frac{p_y}{\sqrt{2\pi}}\right)\left(\frac{\partial u}{\partial y}\right)$.

Using the similarity transformations, we obtain:

$$\left.\begin{aligned} &C_f\;\mathrm{Re}_x^{\frac{1}{2}} = \delta\left(1+\frac{1}{\gamma}\right)f'',\\ &\frac{Nu_x}{\sqrt{\mathrm{Re}_x}} - \theta'(0), \qquad \frac{Sh_x}{\sqrt{\mathrm{Re}_x}} - \phi'(0). \end{aligned}\right\} \quad (13)$$

here, $\mathrm{Re}_x = \frac{U_w x}{\nu}$ is the local Reynold number.

4. Solution Approach

Numerous analytical and numerical techniques, including the homotopy perturbation method, homotopy analysis method, optimised homotopy analysis method, adomian decomposition method, finite difference method, finite element method, etc., can be used to solve the resulting non-linear system of ODEs. We chose the shooting method, a well-known numerical methodology that is an effective strategy in terms of processing time.

The shooting approach has been used to find solutions for various values of the parameters involved in the system of nonlinear ODEs (7–9) subject to boundary constraints (10). Basically, equation (7) is solved numerically and afterward the computed results of f, f' and f'' are used in equations (8)-(9). For the numerical treatment of equation (7), the missing initial condition $f''(0)$ has been denoted as p and the following notations have been considered.

$$\left.\begin{aligned} &f = g_1, f' = g_1' = g_2, f'' = g_1'' = g_2' = g_3,\\ &\frac{\partial f}{\partial p} = g_4, \frac{\partial f'}{\partial p} = g_5, \frac{\partial f''}{\partial p} = g_6. \end{aligned}\right\} \quad (14)$$

The equation (7) can be translated into a scheme of three first-order ODEs using the upward notations. The reduced form of equation (7) is the first three of the ODEs and the remaining three are taken by differentiating the first three w.r.t p .

$$g_1' = g_2, \qquad g_1(0) = 0,$$

$$g_2' = g_3, \qquad g_2(0) = 1 + \delta\left(1 + \frac{1}{\gamma}\right)g,$$

$$g_3' = -\frac{1}{\left(1+\frac{1}{\gamma}\right)}\left[g_2^2 + A^2 - g_1 g_3 - M\,(A - g_2)\right], \qquad g_3(0) = p,$$

$$g_4' = g_5, \qquad g_4(0) = 0,$$

$$g_5' = g_6, \qquad g_5(0)) = \delta\left(1+\frac{1}{\gamma}\right),$$

$$g_6' = \frac{1}{\left(1+\frac{1}{\gamma}\right)}[2g_2 g_5 - g_4 g_3 - g_1 g_6 + M g_5], \qquad g_6(0) = 1,$$

To solve the above initial value problem with Adam's Moulton method of order four, we must take some initial guesses for p . The missing condition for the above system of equations is to be picked to such an extent that $\left(g_2(\infty)\right)_p = A$. Newton's method is utilized to improve these original estimates.

$$p^{(n+1)} = p^{(n)} - \frac{\left(g_2(\eta_\infty)\right)_{g=g^{(n)}} - A}{\left(\frac{\partial g_2(\eta_\infty)}{\partial p}\right)_{p=p^{(n)}}}, \tag{15}$$

The following benchmark is achieved,

$$\left|g_2(\eta_\infty) - A\right| < \varepsilon, \tag{16}$$

To solve the equations (8) and (9), it is converted into the following system of the first order differential expressions and f as a known function. The following notations were therefore taken into consideration.

$$\left.\begin{aligned} &\theta = y_1, \theta' = y_2, \phi = y_3, \phi' = y_4, \frac{\partial\theta}{\partial s} = y_5, \\ &\frac{\partial\theta'}{\partial s} = y_6, \ \frac{\partial\phi}{\partial s} = y_7, \ \frac{\partial\phi'}{\partial s} = y_8, \ \frac{\partial\theta}{\partial t} = y_9, \\ &\frac{\partial\theta'}{\partial t} = y_{10}, \ \frac{\partial\phi}{\partial t} = y_{11}, \ \frac{\partial\phi'}{\partial t} = y_{12}. \end{aligned}\right\} \tag{17}$$

The following resulting system of equations is achieved:

$$\left.\begin{aligned} y_1' &= y_2, & y_1(0) &= s, \\ y_2' &= \frac{-\Pr}{\left(1+\frac{4}{3R}\right)}\left[\begin{array}{l} f\,y_2 + Nb\,y_2\,y_4 + \\ Nt\,y_2^2 + Ec\left(1+\frac{1}{\gamma}\right)\left(f''\right)^2 \end{array}\right], \\ & & y_2(0) &= -Bi(1-s), \\ y_3' &= y_4, & y_3(0) &= 1, \\ y_4' &= -Le\Pr f\,y_4 - \frac{Nt}{Nb}y_2' + Le\,Kr\,y_3, \\ & & y_4(0) &= t, \\ y_5' &= y_6, & y_5(0) &= 0, \\ y_6' &= \frac{-\Pr}{\left(1+\frac{4}{3R}\right)}\left[\begin{array}{l} f\,y_6 \\ +Nb\left(y_4\,y_6 + y_2\,y_8\right) \\ +2\,Nt\,y_2\,y_6 \end{array}\right], \\ & & y_6(0) &= B_i, \\ y_7' &= y_8, & y_7(0) &= 0, \\ y_8' &= -Le\Pr f\,y_8 - \frac{Nt}{Nb}y_6' + Le\,Kr\,y_7, \\ & & y_8(0) &= 0, \\ y_9' &= y_{10}, & y_9(0) &= 0, \\ y_{10}' &= \frac{-\Pr}{\left(1+\frac{4}{3R}\right)}\left[\begin{array}{l} f\,y_{10} + \\ Nb\left(y_4\,y_{10} + y_2\,y_{12}\right) \\ +2\,Nt\,y_2\,y_{10} \end{array}\right], \\ & & y_{10}(0) &= 0, \\ y_{11}' &= y_{12}, & y_{11}(0) &= 0, \\ y_{12}' &= -Le\Pr f\,y_{12} - \frac{Nt}{Nb}y_{10}' + Le\;Kr\,y_{11}, \\ & & y_{12}(0) &= 1, \end{aligned}\right\} \tag{18}$$

Now eq. (18) can solve numerically with the help of Shooting technique along with Adam's-Moulton method. To get the approximate solution, the domain of the problem has been taken as $[0, \eta_\infty]$ instead of $[0, \infty)$, where η_∞ is an appropriate finite positive real number. In the above system of equations, the missing conditions s and t , must be chosen in such a way that,

$$h_2(\eta_\infty, s, t)_s = 0, \qquad h_4(\eta_\infty, s, t)_s = 0 \tag{19}$$

For the improvement of the missing condition, Newton's method has been implemented which is conducted by the following iterative scheme:

$$\begin{bmatrix} s^{(k+1)} \\ t^{(k+1)} \end{bmatrix} = \begin{bmatrix} s^{(k)} \\ t^{(k)} \end{bmatrix} - \left[\begin{bmatrix} h_7 & h_9 \\ h_{11} & h_{14} \end{bmatrix}^{-1} \begin{bmatrix} h_2 \\ h_4 \end{bmatrix} \right]_{\left(s^{(k)}, t^{(k)}, \eta_\infty\right)} \quad (20)$$

The following steps are involved for the accomplishment of the shooting method.

(i). Choice of the guesses $s = s^{(0)}$ and $t = t^{(0)}$

(ii). Choice of a positive small number ε.
If $\max\left\{\left|\left(y_1(\eta_\infty)\right)\right|, \left|\left(y_3(\eta_\infty)\right)\right|\right\} < \varepsilon$, the process is terminated, otherwise go to (iii)

(iii). Compute $r^{(k+1)}$ and $s^{(k+1)}$, $k = 0, 1, 2, ..$ by using equation (20).

(iv). Repeat (i) and (ii).
All through this article, ε has been taken as 10^{-12} while η_∞ is set as 7.

5. Analysis of Results

This section addresses the numerical solutions in detail, using graphs and tables. This will primarily address the velocity, temperature, and concentration profile. The present results will be compared with those of [20] for verification of the code. The numerical calculations are executed for the observation of the impact of various parametric values of γ, δ, A, Bi, Nb, Nt, Le, Kr on velocity, temperature, mas fraction field.

In Table 1, comparison of Skin Friction Coefficient $-f''(0)$ for different values of δ is displayed. The results were compared with those obtained by Hayat et al. [13] and Ibrahim and Makinde. [20] and found both to be in excellent agreement. From table 1 it is observed that skin friction coefficient is decreased by increase of slip parameter.

Table 2 shows the skin-friction coefficient $-f''(0)$ decreases by the increase of A. The effect of δ on Nusselt number $-\theta'(0)$ decreases and Sherwood number $-\phi'(0)$ is opposite as compared to Nusselt number.

Table 1. Comparison of the values of Skin Friction Coefficient $-f''(0)$ those from Ibrahim and Makinde [25].

δ	Hayat et al. [13]	Ibrahim and Makinde [25]	Present study
0.0	1.000000	1.0000	0 .9999855
0.1	0.872082	0.8721	0.8720812
0.2	0.776377	0.7764	0.7763964
0.5	0.591195	0.5912	0 .5912748
2.0	0.283981	0.2840	0 .2841796
5.0	0.144841	0.1448	0 .1450588
10.0	0.081249	0.0812	0 .0814330
20.0	0.043782	0.0438	0 .0439329
50.0	0.018634	0.0186	0 .0186789

Table 2. Comparison of numerical values of Skin Friction coefficient $-f''(0)$, Local Nusselt number $-\theta'(0)$ and Local Sherwood number $-\phi'(0)$ those from Ibrahim and Makinde [25].

A	δ	γ	$-f''(0)$		$-\theta'(0)$		$-\phi'(0)$	
			Ibrahim and Makinde [25]	Present study	Ibrahim and Makinde [25]	Present study	Ibrahim and Makinde [25]	Present study
0.0	0.1	10	1.1451	1.1414830	0.0922	0.0921669	2.0435	2.0434700
0.1			1.0653	1.0653210	0.0923	0.0923036	2.0849	2.0848620
0.2			0.9792	0.9791939	0.0924	0.0924430	2.1283	2.1282550
0.3			0.8838	0.88382410	0.0926	0.0925826	2.1730	2.1730430
0.9			0.1467	0.1466890	0.0934	0.0933622	2.4534	2.4533620
1.5			-0.818	-0.8188152	0.0940	0.0940005	2.7333	2.7333010
2.0			-1.762	-1.7622860	0.0944	0.0944359	2.9597	2.9597170
2.4			-2.594	-2.5944010	0.0947	0.0947337	3.1356	3.1356140
0.4	0.2		0.6758	0.6757960	0.0925	0.0924937	2.1478	2.1477870
	0.4		0.5357	0.5356795	0.0921	0.0921433	2.0464	2.0464120
	0.6		0.4449	0.4449050	0.0919	0.0918827	1.9768	1.9767530
	0.8		0.3810	0.0934260	0.0917	0.0916797	1.9256	1.9255770
	0.4	0.1	0.0908	0.0907876	0.0916	0.0915679	1.9015	1.9014960
		0.5	0.2563	0.2563434	0.0920	0.0919709	2.0018	2.0018460
		1	0.3477	0.3477455	0.0921	0.0920584	2.0246	2.0245580
		10	0.5357	0.5356796	0.0921	0.0921433	2.0464	2.0464120
		100	0.5688	0.5688785	0.0921	0.0921503	2.0482	2.0481280

Table 3. Behaviour of $-f''(0)$, $-\theta'(0)$ and $-\phi'(0)$ for variable values of A, δ, γ, Nb, Nt, Pr, Le, Bi, M.

A	δ	γ	Nb	Nt	Pr	Le	Bi	M	$-f''(0)$	$-\theta'(0)$	$-\phi'(0)$
0.0	0.1	10	0.1	0.1	10	10	0.1	1.0	1.1415110	0.08939873	7.211071
0.1									1.0653300	0.08959904	7.270552
0.2									0.9791964	0.08980191	7.336496
0.3									0.8838250	0.09000381	7.408033
0.9									0.1466889	0.09113192	7.920059
1.5									-0.8188149	0.09200104	8.511965
2.0									-1.7622840	0.09259528	9.032217
2.4									-2.5944000	0.09301120	9.456006
0.4	0.2								0.67579670	0.08990348	7.230251
	0.4								0.53567970	0.08944395	6.864066
	0.6								0.44490520	0.08910342	6.609847
	0.8								0.38096870	0.08883907	6.421543
	0.4	0.1							0.09215718	0.08866987	6.154168
		0.5							0.25656680	0.08923871	6.594784
		1							0.34781170	0.08934746	6.712249
		10							0.53568420	0.08944392	6.864055
		100							0.56880820	0.08945096	6.883239

Table 3 shows the numerical results of the skin-friction coefficient along with the Nusselt and Sherwood numbers for the current model in respect of a shift in the values of various parameters such as A, δ, γ, Nb, Nt, Pr, Le, Bi, M. From the results, it was noted that the skin-friction coefficient decreases for the larger values of A and δ, while heat and mass transfer rates increase significantly.

Figure 2 is drawn to investigate the effect of Casson parameter on the velocity filed. The fluid velocity increases with an increasing value of Casson parameter (γ). Physically, the consistency of the fluid increments due to the escalation of γ the values and then decreases, the fluid's velocity profile also decreases the velocity boundary layer thickness for uprising values of Casson parameter (γ). Furthermore, the present phenomenon changes to Newtonian fluid when γ tends to infinity.

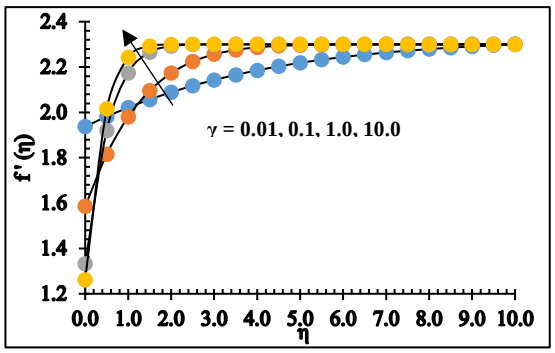

Fig. 2. Influence of Casson parameter on axial velocity profile when $\delta = 0.1, A = 2.3, M = 1$.

Figure 3 reveals the impact of Casson Parameter (γ) on temperature distribution. The escalating values of γ by which the mounting values of temperature depiction. Generally, the thermal boundary layer depth uprise by increasing values of γ due to which the surface temperature enlarges with.

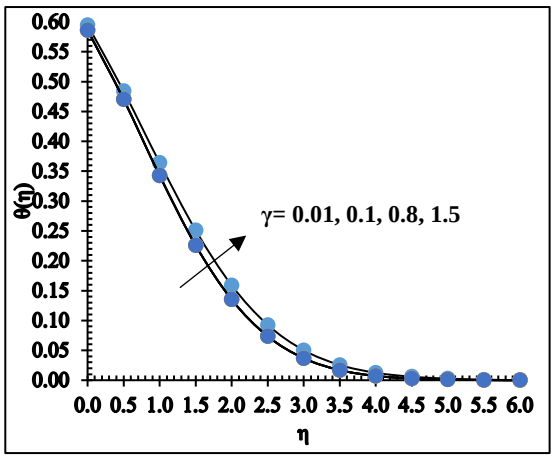

Fig. 3. Influence of Casson parameter on temperature profile when $Nt = Nb = 0.5, Le = 2, A = 0.4,\ \mathrm{Pr} = M = 1$ $Bi = 0.5, \delta = R = Ec = 0.2,$

Figure 4 indicates the impact of δ on the distribution of dimensionless velocity. It is clearly shown that by an enhancing value of the velocity profile arises. Generally, the growing values of δ create a frictional resistance between the surface of the sheet and fluid particles escalates, which causes a decrement of the fluid velocity.

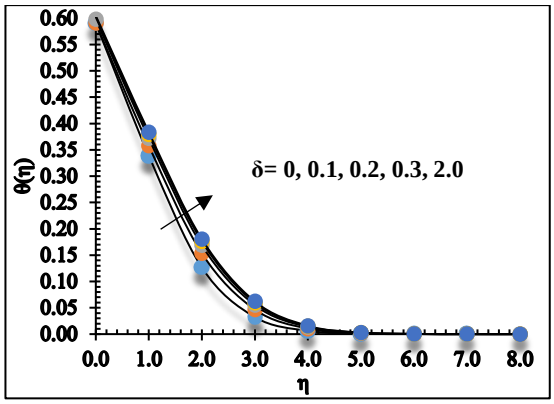

Fig. 4. Influence of momentum slip on axial velocity profile when $\gamma = 0.1, A = 0.4, M = 1.$

Figure 5 illustrates the influence of δ on temperature distribution, from the figure it is apparent that especially for cautiously enlarging values of δ, the temperature field is enhanced. Increasing the values of δ the thermal boundary layer depth also raises the sheet surface temperature.

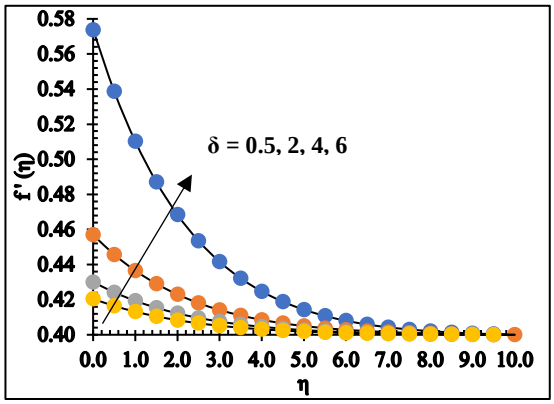

Fig. 5. Impact of momentum slip on temperature profile when $Nt = Nb = 0.5, Le = 2, \gamma = 0.1, Bi = 0.5,$ $R = Ec = 0.2, \Pr = M = 1, A = 0.4.$

Figure 6 analyses the effect of A on the distribution of dimensionless velocity. From the figure it is apparent that when the free stream velocity is greater than the surface velocity, while the fluid particle velocity accelerates at $A > 1$. In addition, the thickness of the boundary layer decelerates by increasing the A values. In fact, if the stretching velocity is less than the free-stream velocity the velocity graph tends to be A . Often, when the extending sheet velocity is greater than the free-stream velocity, which creates a fluid velocity declaration.

Figure 7 displays the effect of A on temperature distribution. As the value A heightens, the heat transfer from the sheet to the fluid become smaller and as a result, the temperature falls significantly. Furthermore the thermal boundary layer thickness id reduced.

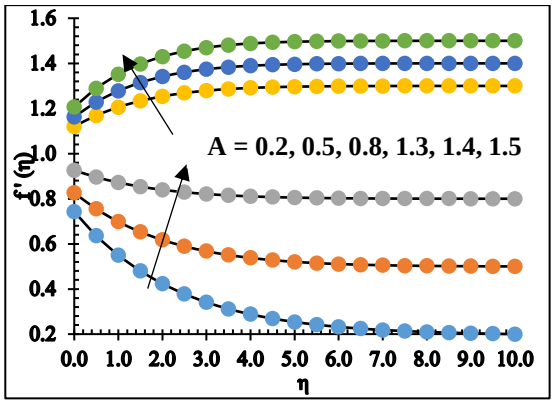

Fig. 6. Impact of A on axial velocity profile when $\gamma = 0.1, \delta = 0.1, M = 1.$

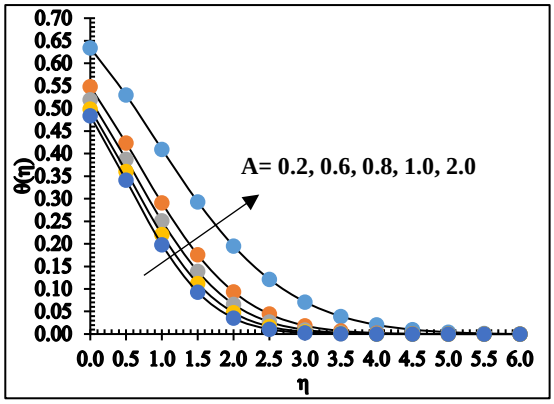

Fig. 7. Influence of on temperature profile when $Le = 2,$ $Nt = Nb = 0.5, \ \gamma = 0.1, Bi = 0.5, \delta = R = E_C = 0.2, \Pr = M = 1.$

Figure 8 reflects the influence of Boit number on the dimensionless temperature distribution. The graph of the velocity profile specifies that an increment in Bi causes an enhancement in the temperature profile. Generally, Biot number is expressed as the ratio of temperature change at the surface to conduction within the surface of the body. As expected, the boosting values of Bi enhanced the thermal boundary layer of the fluid.

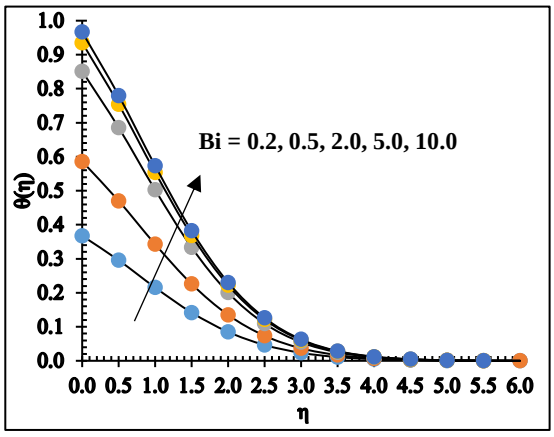

Fig. 8. Influence of temperature slip on temperature profile when $Nt = Nb = 0.5, Le = 2, \gamma = 0.1, \Pr = M = 1,$ $\delta = 0.2, A = 0.4.$

Figure 9 manifests the relationship between Bi (Biot number) and the concentration profile. For boosting values of Biot number the graph of dimensionless concentration profile is increased. Increasing Bi means a decrement in the fluid's conductivity because of which the boundary layer of concentration is increased.

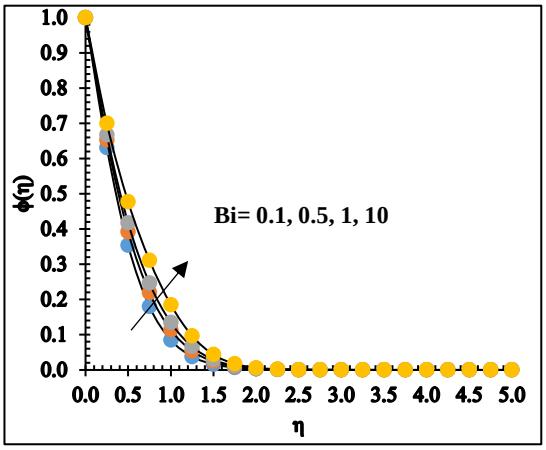

Fig. 9. Influence of Biot number on nanoparticle volume fraction profile when $Nt = Nb = 0.1, \Pr = 5, A = 0.4,\ \delta = 0.1,$ $\gamma = R = Ec = 0.2, Le = M = 1.$

Figure 10 illustrates the Nt effect on temperature distribution. From the figure it is transparent that the $\theta(\eta)$ field is improved for moderately enlarging values of Nt. In addition, the particles Nt apply a force on the other particles because of which these particles shift from the hotter to less region. Therefore, there is an intensification of the fluid's $\theta(\eta)$ profile.

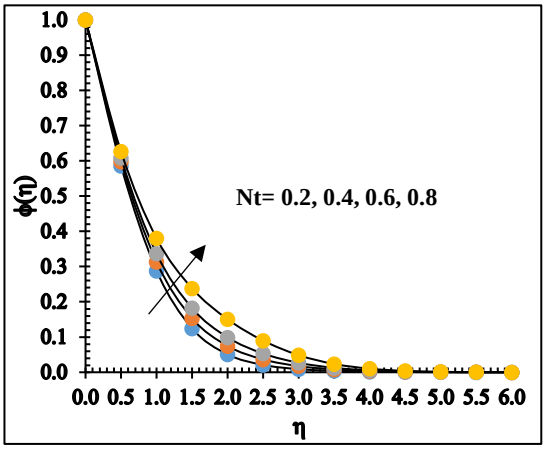

Fig. 10. Influence of Nt on temperature profile when $Nb = 0.5, Le = 2, \gamma = 0.1, Bi = 0.5, \delta = R = Ec = 0.2,$ $\Pr = M = 1,\quad A = 0.4.$

Figure 11 illustrates the impact of Nt on concentration distribution, from the figure for gradually enlarging values of Nt the concentration field is enhanced.

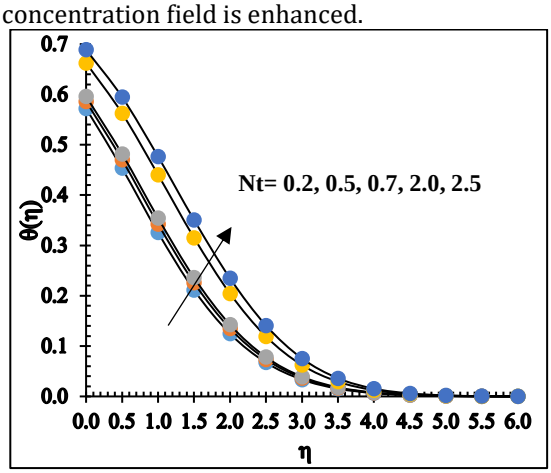

Fig. 11. Influence of Nt on nanoparticle volume fraction profile when $Nb = 0.1, \Pr = 5, A = 0.4,\ \delta = 0.1, Le = M = 1,$ $Bi = \gamma = R = Ec = 0.2.$

Figure 12 analyses the impact of Brownian motion parameter on the temperature distribution. The temperature profile climbs marginally for the large values of Nb. This happens due to the reason that as the value of Brownian motion parameter rises, the movement of the nanoparticle enhances significantly which triggers the kinetic energy of the nanoparticles and eventually, the temperature enhances, and thermal boundary layer thickness is magnified.

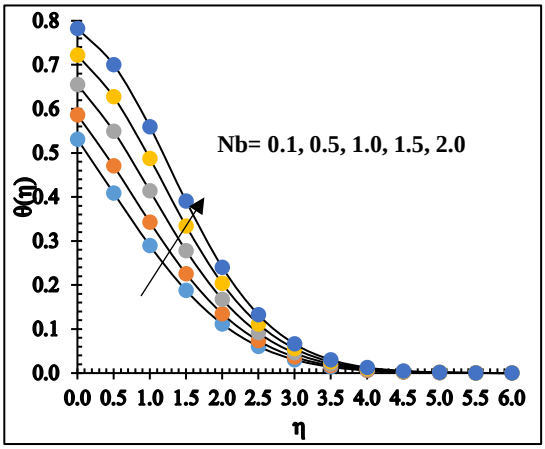

Fig. 12. Influence of Nb on temperature profile when $Nt = 0.5, Le = 2, \gamma = 0.1, Bi = 0.5, \delta = R = Ec = 0.2,$ $\Pr = M = 1, A = 0.4.$

Figure 13 shows the connection between Lewis numbers and the dimensional concentration distribution. Concentration profile decelerates for the boosting values of Lewis number (Le), physically Lewis number express the respective contribution of rate of thermal diffusion to the rate of species diffusion on the

boundary region. As increasing values of Lewis number (Le).

Figure 14 portrays the impact of Eckert number on the temperature field. It is noticed that there is a gradual decrease in the fluid energy by an increment in Ec. Here, it is observed that the temperature increases for gaining the values of Ec. Physically, the Eckert number depicts the relation between the kinetic energy of the fluid particles and the boundary layer enthalpy. The kinetic energy of the fluid particles rises as Ec assume the large values. Hence, the temperature of the fluid climbs marginally and therefore, the associated thermal boundary layer thickness is enhanced.

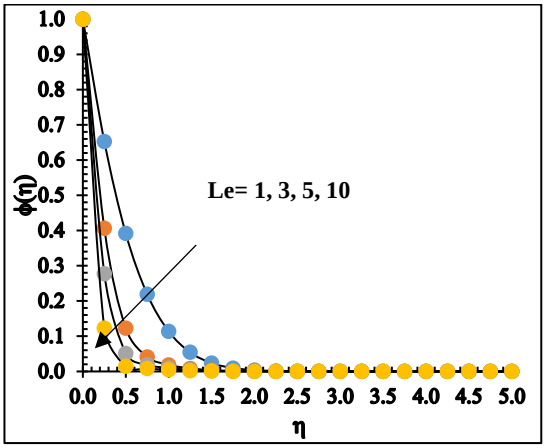

Fig. 13. Influence of Lewis number on nanoparticle volume fraction profile when $Nt = Nb = Bi = 0.1, \Pr = 5,\ \delta = 0.1,$ $A = 0.4,\ \gamma = R = Ec = 0.2, M = 1.$

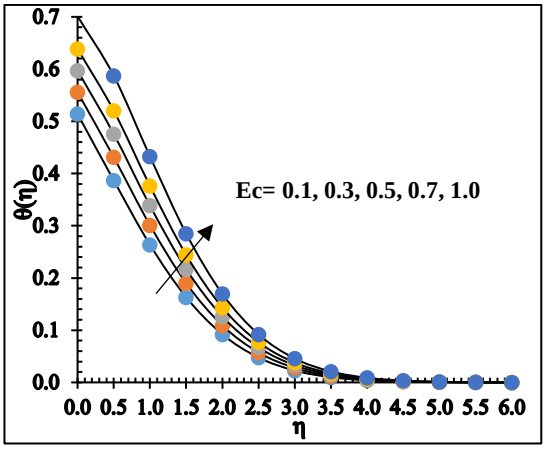

Fig. 14. Influence of Eckert number on temperature profile when $Nt = Nb = 0.2 \Pr = 5, A = 0.4,\ \delta = 0.1, Bi = 0.2,$ $\gamma = R = 0.2,\ Le = M = 1.$

Figure 15 is sketched for the investigation of the temperature profile in response to the thermal radiation parameter R. By increasing the thermal radiation, increase in temperature profile is observed. Physically, a magnification in provides additional heat to the operating fluid which amplifies the temperature field.

Figure 16 shows the effects of chemical reaction parameter on the concentration field $\phi(\eta)$. It is noticed that Increasing values of chemical reaction parameter concentration as well as the thickness of concentration decreases. It is because of the fact that the chemical reaction in this system results in chemical dissipation and therefore results in decreases in the profile of concentration. The most significant influence is that chemical reaction tends to decrease the overshoot in the concentration profile and their associated boundary layer.

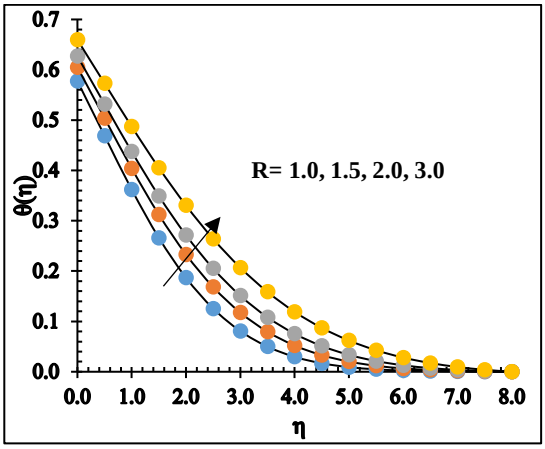

Fig. 15. Influence of Radiation parameter on temperature profile when $Nt = Nb = 0.2 \Pr = 5, A = 0.4,\ \delta = 0.1,\ Bi = 0.2,$ $\gamma = Ec = 0.2, Le = M = 1.$

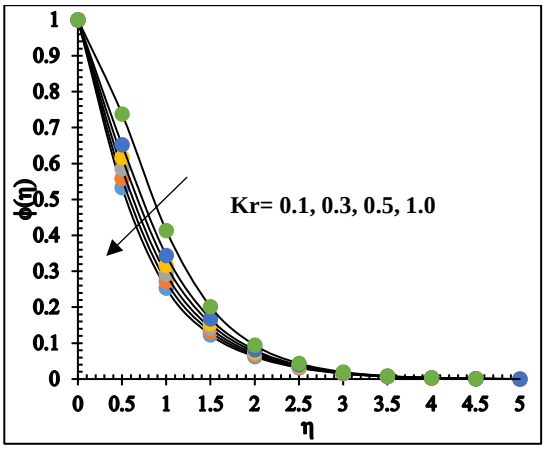

Fig. 16. Influence of Chemical reaction on nanoparticle volume fraction profile when $Nt = Nb = 0.2, \Pr = 0.5,$ $A = 0.4,\ \delta = 0.1, Bi = \gamma = Ec = 0.2, Lr = M = 1, R = 0.2.$

6. Conclusions

This article presented numerical simulations of boundary layer flow of Casson nanofluid over a linear stretching sheet in the presence of chemical reaction with slip conditions on the flow field. We applied suitable similarity

transformations to reduce the complex governing equations into a set of ODEs. The numerical solutions are obtained by using the shooting method with Adams Moulton method. Our results are excellent agreement with the existing numerical literature results. Different physical parameters are inspected on fluid flow: heat transfer and mass transfer characteristics. In light of the numerical results, the following keynotes are made.

- The fluid velocity declines with increasing values of Casson and slip parameter.
- The fluid energy accelerates effectively with an increase in the Biot number.
- The temperature distribution enhances effectively with uprising values of Brownian motion and thermophoresis parameters.
- Concentration profile decelerates for the boosting values of Lewis number and thus we get a small molecular diffusivity and thermal boundary layer.
- Fluid concentration and associative boundary thickness are increasing functions of Casson parameter.
- The thermal boundary layer thickness increases for the rise of Eckert number (Ec) as well as radiation parameter (R).
- Higher values of chemical reaction (Kr) leading to a reduction in nanoparticle concentration.
- It is noted that Nu_x is also increased by enhancing the values of Lewis number (Le) .
- The problem can be extended for stretching surface in different types of fluids for instance Maxwell nanofluid Carreau nanofluid.
- Different numerical techniques can be utilized to solve fluid flow problems.

Nomenclature

The following symbols are used in this paper:

$a,\ b$ Stretching constant $\left(s^{-1}\right)$

B_0 Magnetic field strength $\left(Wbm^{-2}\right)$

D_B Brownian diffusion coefficient

D_T Thermophoretic diffusion coefficient

κ Thermal conductivity $\left(Wm^{-1}K^{-1}\right)$

$\sigma^{\bullet}$ Stefan-Boltzmann constant $\left(kg\ m^{-2}K^{-4}\right)$

$\kappa^{\bullet}$ Mean absorption coefficient

Ec Eckert number

Le Lewis number

M Magnetic parameter

N_b Brownian motion parameter

N_t Thermophoresis parameter

Nu Nusselt number

Nu_x Reduced Nusselt number

Pr Prandtl number

p Pressure

c_f Heat capacity of the fluid $\left(Jm^{-3}K^{-1}\right)$

c_p Effective heat capacity of the nanoparticle material $\left(Jm^{-3}K^{-1}\right)$

q_r Radiative heat flux $\left(kg\ m^{-2}\right)$

q_m Wall mass flux $\left(W\,m^{-2}\right)$

q_w Wall heat flux $\left(W\,m^{-2}\right)$

Re_x Local Reynolds number

Shr Reduced Sherwood number

Sh_x Local Sherwood number

T Fluid temperature (K)

T_w Temperature at the stretching sheet (K)

T_∞ Ambient temperature (K)

u, v Velocity components along $x-$ and $y-$ axis $\left(m.s^{-1}\right)$

u_w Velocity of the stretching sheet $\left(m.s^{-1}\right)$

x, y Cartesian coordinates ($x-$ axis is aligned along the stretching surface and $y-$ axis is normal to it) (L)

α Thermal diffusivity $\left(m^2\ s^{-1}\right)$

ϕ Dimensionless nanoparticle volume fraction

η Similarity variable

ψ Stream function $\left(m^2\ s^{-1}\right)$

θ Dimensionless temperature

ρ_f Fluid density $\left(kg\ m^{-3}\right)$

ρ_p Nanoparticle mass density $\left(kg\ m^{-3}\right)$

σ Electrical conductivity of the fluid

τ Parameter defined by ratio between the effective heat capacity of the nanoparticle material and heat capacity of the fluid. $\tau = (\rho c)_p / (\rho c)_f$

Acknowledgments

The authors wish to express their very sincere thanks to the referees for their valuable comments and suggestions.

Funding Statement

This research received no specific grant from any funding agency in the public, commercial, or not-for-profit sectors.

Conflicts of Interest

The author declares that there is no conflict of interest regarding the publication of this article.

References

[1] M. Jamil and C. Fetecau, 2010. Some exact solutions for rotating flows of a generalized Burgers fluid in cylindrical domains. *Journal of Non-Newtonian Fluid Mechanics*, 165(23-24), pp. 1700-1712. doi: 10.1016/j.jnnfm.2010.08.004

[2] M. M. Rashidi, M. M. Bhatti, M. A. Abbas, and M. E.-S. Ali, 2016. Entropy generation on MHD blood flow of nanofluid due to peristaltic waves. *Entropy*, 18(4), pp. 117. Doi: https://doi.org/10.3390/e18040117

[3] E. V. Goncalves and S. C. Lannes, 2010. Chocolate rheology. *Food Science and Technology*, 30(4), pp. 845-851. Doi:https://www.redalyc.org/articulo.oa?id=395940102002

[4] G. Narender, K. Govardhan and G. Sreedhar Sarma, 2020. Magnetohydrodynamic stagnation point on a Casson nanofluid flow over a radially stretching sheet. *Beilstein J. Nanotech nol.*, 11, pp. 1303–1315. Doi: https://doi.org/10.3762/bjnano

[5] G. Narender, K. Govardhan and G. Sreedhar Sarma, 2021. MHD Casson Nanofluid Past a Stretching Sheet with the Effects of Viscous Dissipation, Chemical Reaction and Heat Source/Sink. *J. Appl. Comput. Mech.,* 7(4), pp. 2040–2048. doi: 10.22055/JACM.2019.14804

[6] Govardhan K, Narender G, Sarma GS, 2019. Viscous dissipation and chemical reaction effects on MHD Casson nanofluid over a stretching sheet. *Malaysian Journal of Fundamental and Applied Sciences*, 15(4), pp. 585–592. doi: 10.11113/mjfas.v15n4.1256

[7] Elelamy, A.F., Elgazery, N.S. and Ellahi, R., 2020. Blood flow of MHD non-Newtonian nanofluid with heat transfer and slip effects: Application of bacterial growth in heart valve. *International Journal of Numerical Methods for Heat & Fluid Flow*, 30(11), pp. 4883-4908. doi: https://doi.org/10.1108/HFF-12-2019-0910

[8] M.A. Yousif, H.F. Ismael, T. Abbas, R. Ellahi, 2019. Numerical study of momentum and heat transfer of MHD Carreau nanofluid over exponentially stretched plate with internal heat source/sink and radiation. *Heat Transf. Res.*, 50(7), pp. 649-658. doi: 10.1615/HeatTransRes. 2018025568

[9] Zeeshan, A.; Khan, M.I.; Ellahi, R.; Marin, M., 2023. Computational Intelligence Approach for Optimising MHD Casson Ternary Hybrid Nanofluid over the Shrinking Sheet with the Effects of Radiation. *Appl. Sci.*, 13, pp. 9510.

doi: https://doi.org/10.3390/app13179510

[10] M. Sheikholeslami, M. Gorji-Bandpy, and D. Ganji., 2014. Lattice Boltzmann method for MHD natural convection heat transfer using nanofluid. *Powder Technology*, 254, pp. 82-93. doi: https://doi.org/10.1016/j.powtec.2013.12.054

[11] M. Rashidi, N. V. Ganesh, A. A, Hakeem, and B. Ganga., 2014. Buoyancy effect on MHD flow of nanofluid over a stretching sheet in the presence of thermal radiation. *Journal of Molecular Liquids*, 198, pp. 234-238. doi:https://doi.org/10.1016/j.molliq.2014.06.037

[12] A. Zeeshan, A. Majeed, and R. Ellahi, 2015. Effect of magnetic dipole on viscous ferro-fluid past a stretching surface with thermal radiation. *Journal of Molecular liquids*, 215, pp. 549-554. doi: https://doi.org/10.1016/j.molliq.2015.12.110

[13] T. Hayat, S. Asad, M. Mustafa, and A. Alsaedi, 2015. MHD stagnation-point flow of Jeffrey fluid over a convectively heated stretching sheet. *Computers & Fluids*, 108, pp. 179-185. doi:https://doi.org/10.1016/j.compfluid.2014.11.016

[14] G. Narender, K. Govardhan and G. Sreedhar Sarma, 2021. Viscous dissipation and thermal radiation effects on the flow of Maxwell nanouid over a stretching surface. *Int. J. Nonlinear Anal. Appl.*, 12(2), pp. 1267-1287, doi:10.22075/ijnaa.2020.18958.2045

[15] R. Ellahi, 2013. The effects of MHD and temperature dependent viscosity on the flow of non-Newtonian nanofluid in a pipe: Analytical solutions. *Applied Mathema'tical Modelling*, 37, pp.1451–1467. doi: http://dx.doi.org/10.1016/j.apm.2012.04.004.

[16] Majeed A, Zeeshan A, Alamri SZ, Ellahi R, 2018. Heat transfer analysis in ferromagnetic viscoelastic fluid flow over a stretching sheet with suction. *Neural Comput & Applic*, 30(6), pp.1979-1955. doi: https://doi.org/10.1007/s00521-016-2830-6.

[17] S. Shah, S. Hussain, and M. Sagheer, 2016. MHD effects and heat transfer for the UCM fluid along with Joule heating and thermal radiation using Cattaneo-Christov heat flux model. *AIP Advances*, 6, doi: https://doi.org/10.1063/1.4960830

[18] M. Madhu, N. Kishan, and A. J. Chamkha, 2017. Unsteady flow of a Maxwell nanofluid over a stretching surface in the presence of magnetohydrodynamic and thermal radiation effects. *Propulsion and Power Research*, 6, pp. 31-40, doi: https://doi.org/10.1016/j.jppr.2017.01.002

[19] M. F. Endalew and A. Nayak, 2018. Thermal radiation and inclined magnetic field effects on MHD flow past a linearly accelerated inclined plate in a porous medium with variable temperature. *Heat Transfer-Asian Research*, 48(4), pp. 1-20. doi: 10.1002/htj.21367

[20] Chaoli Zhang, Liancun Zhang, Xinxin Zhang and Goong Chen., 2015. MHD Flow and radiation heat transfer of nanofluids in porous media with variable surface heat flux and chemical reaction. Applied Mathematical Modelling, 39(9), pp. 165 – 181. doi:https://doi.org/10.1016/j.apm.2014.05.023

[21] Gobburu Sreedhar Sarma, Ganji Narender, Kamatam Govardhan, 2022. Radiation effect on the flow of Magneto Hydrodynamic nanofluids over a stretching surface with Chemical reaction, *Journal of Computational Applied Mechanics*, 53(4), pp. 494-509. doi: 10.22059/JCAMECH.2022.348047.749

[22] Batcha Srisailam, Katkoori Sreeram Reddy, Ganji Narender and Bala Siddhulu Malga, 2023. The Effect of Viscous Dissipation and Chemical reaction on the flow of MHD Nanofluid. *Journal of Advanced Research in Fluid Mechanics and Thermal Sciences*, 107(2), pp. 150-170. doi: https://doi.org/10.37934/arfmts.107.2.150170

[23] M.H. Yazdi, S. Abdullah, I. Hashim, K. Sopian, 2011. Slip MHD liquid flow and heat transfer over non-linear permeable stretching surface with chemical reaction. *International Journal of Heat and Mass Transfer,* 54, pp. 3214–3225. doi:https://doi.org/10.1016/j.ijheatmasstransfer.2011.04.009

[24] Daniel, Y.S., Aziz, Z.A., Ismail, Z., Salah, F., 2017. Entropy analysis in electrical magnetohydrodynamic (MHD) flow of nanofluid with effects of thermal radiation, viscous dissipation and Chemical reaction. *Theor. Appl. Mech. Lett*., 7(4), pp. 235-242. doi:https://doi.org/10.1016/j.taml.2017.06.003.

[25] W. Ibrahim and O. Makinde, 2015. Magnetohydrodynamic stagnation point flow and heat transfer of Casson nanofluid past a stretching sheet with slip and convective boundary condition. *Journal of Aerospace Engineering,* 29(2), pp. 04015037. doi:10.1061/(ASCE)AS.1943-5525.0000529